

A New Variational Model with Dual Level Set Functions for Selective Segmentation

Lavdie Rada and Ke Chen*

Centre for Mathematical Imaging Techniques (CMIT) and Department of Mathematical Sciences, The University of Liverpool, Peach Street, Liverpool L69 7ZL, United Kingdom.

Received 19 January 2011; Accepted (in revised version) 21 June 2011

Available online 30 January 2012

Abstract. In this paper we present a selective segmentation model using a dual level set variational formulation. Our variational model aims to segment all objects with one level set function (global) and the selected object, which is the closest to the geometric constraints (markers), with another level set (local). It is a combination of edge detection, markers distance function and active contour without edges. Experimental results show that our model is more robust than previous work.

AMS subject classifications: 62H35, 65N22, 65N55, 74G65, 74G75

Key words: Image selective segmentation, level set function, Euler-Lagrange equation, 2D image segmentation, re-initialization.

1 Introduction

Image segmentation is a central problem among image processing applications. Its aim is to distinguish objects in the image foreground from background and to systematically select specific features out of an image that has many features.

There are different techniques developed for this task such as histogram analysis and thresholding [21, 29, 32], region growing [2, 35], edge detection and active contours [3, 11, 16]. Active contour models are widely used in image segmentation due to their robustness and reliability. These models are formulated as energy minimization problems and can be categorized broadly into edge-based models [6, 16–18], and region-based models [9, 11, 24, 26, 31]. Edge-based models use the edge information (certain form of gradients) guiding the active contours towards the object boundary, and the region based ones make use of image intensities (certain homogeneity) to guide the motion of active contours.

*Corresponding author. *Email addresses:* ladirada@liv.ac.uk (L. Rada), k.chen@liv.ac.uk (K. Chen)

The above image segmentation models are useful for various applications when all features in the whole image are to be segmented. This challenging task is continually tackled by more refined models but is not required in some other applications such as CCTV monitoring of a subject and medical imaging of a particular organ. For the latter applications, the problem becomes selective segmentation.

The main challenge in a selective image segmentation problem is how to differentiate one feature from another, especially when two objects have similar or same intensities. For example, in an artificial image like in Fig. 1 the intensities between the triangle and the rectangle have an extremely small difference and we might be interested in selecting only one of them. Another example is with medical images (CT and MRI) which often have less contrast in image intensities.

Recent work by Gout and Guyader [14] and Badshah-Chen [4] proposed two different variational models for selective segmentation. The Gout-Guyader model [14, 15] is based on edge information of the object while the Badshah-Chen model [4] combines an edge based model with region based information. Both models are useful and can segment a range of images, but there are cases which appear too challenging for either model. The latter model, with the help of region information, improved the former in robustness and segmentation quality in case of noisy images. It should be remarked that for global segmentation, the idea of combining an edge based model with region based information was earlier used in [5, 30]. However we have observed that the particular selective segmentation model of [4] partly based on Chan-Vese model [11], when solved in a time-marching framework, can reproduce the same solution of two piecewise constants as the Chan-Vese model [11]; if this happens, the capability of selectiveness is lost and we obtain a global segmentation which is not needed for our purpose. This problem is illustrated in the top two plots of Fig. 2 (which solves the problem from Fig. 1).

To further improve on the Badshah-Chen work [4] here we will introduce a new model which does two tasks at the same time, one to find the segmentation of all boundaries and the other to focus on the selected object, which is the closest to the geometric constraints (or markers). The first task implements a global segmentation like a region based model while the second one implements a local segmentation using both local edge and local region information. Since each task is characterized by a level set function [1, 7, 10, 17, 23, 25, 28], our model employs two level set functions, namely, the global function ϕ_G and the local function ϕ_L . Once our dual level set variational model is solved, the global level set function ϕ_G will segment the entire domain while the local one will define the desired selective object. However, since a level set function is not unique away from a boundary, a re-initialization might be required. There are two different techniques of re-initialization, either by solving a re-initialization equation [25] or by incorporation of a functional into the minimization problem [18]. Before proceeding, to give an early clue on our new model to be presented shortly, the bottom two plots of Fig. 2 show our new and correctly segmented results.

We remark that our proposed model for local and selective segmentation may be further speeded up by using the numerical methodology as developed by Sethian [27],

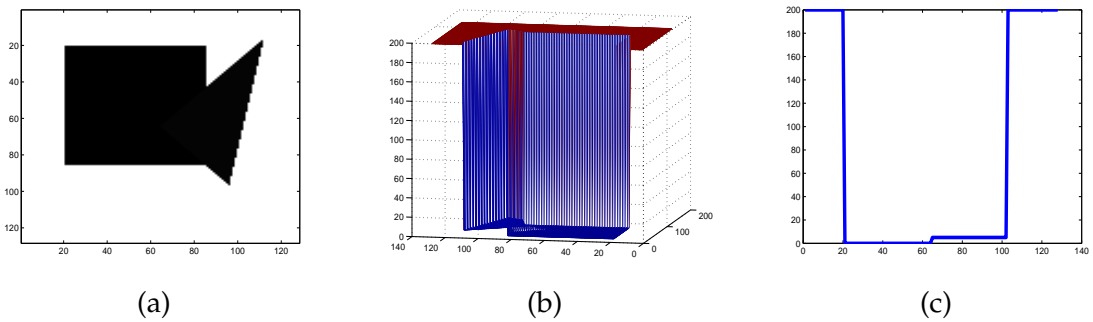


Figure 1: (a) An image of a 2D triangle over a rectangle; (b) Plot of intensities of the image; (c) Plane cut view through the vertical middle of the image.

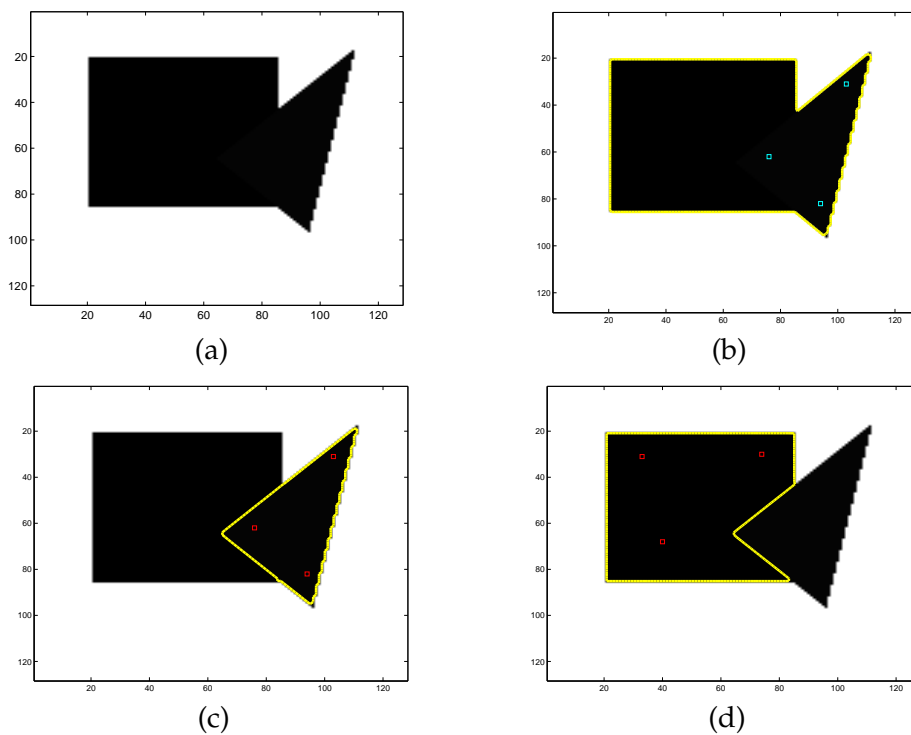


Figure 2: Comparison of (c) by the new model and (b) by an old model of [4]. (a) given image; (b) incorrect result by the old model; (c) correct selection of the triangle by the new model; (d) correct selection of the rectangle by the new model.

known as fast marching methods, which were later extended in Farcadel-Guyader-Gout [12], through evolving boundary contours in a neighbourhood of the underlying zero level set curves.

The rest of this paper is organized in the following way: Section 2 gives a review of existing and related models of Chan-Vese [11], Badshah-Chen [4], and Li-Xu-Gui-Fox [18].

In Section 3 we present the proposed new model and derive the Euler-Lagrange equation. In Section 4 we describe an additive operator splitting method (AOS) for solving the PDE. In Section 5 we give some experimental results to further illustrate the improved robustness of our new model.

2 Review of existing variational segmentation models

As mentioned, there exist many variational segmentation models in the literature [8, 19, 22]. We shall only review three models below that are directly related to this work.

2.1 Chan-Vese model

The Chan-Vese variational model [11] of active contours without edges has been used successfully for segmentation of all image features. This model does not use the gradient of the image as a stopping process as it is a region based method and the stopping term is depending on the Mumford and Shah segmentation technique [24].

The basic idea of the model is as follows. Assume that a given image z is formed by two regions of approximately piecewise constant intensities, of distinct values z_i and z_o and that the object to be detected is represented by the region with intensities closest to the value z_i . Let Γ denote the boundary that separates the two regions Ω_1 and $\Omega_2 = \Omega \setminus \overline{\Omega_1}$. Then $z \approx z_i$ inside the object (inside Γ) and $z \approx z_o$ outside the object (outside Γ). Chan and Vese [11] proposed the variational problem

$$\inf_{c_1, c_2, \Gamma} F(\Gamma, c_1, c_2) \quad (2.1)$$

for the segmentation of all image features, where

$$F(\Gamma, c_1, c_2) = \mu \text{length}(\Gamma) + \lambda_1 \int_{\text{inside}(\Gamma)} |z(x, y) - c_1|^2 dx dy + \lambda_2 \int_{\text{outside}(\Gamma)} |z(x, y) - c_2|^2 dx dy. \quad (2.2)$$

Here $z(x, y)$ is the original image, c_1 and c_2 are the average values of z inside and outside of the variable contour Γ , also μ , λ_1 and λ_2 are non-negative fixed parameters that should be related to the features' diameter. As both the integral and the limits of integration in equation (2.2) are not known, to overcome this problem, a level set function is introduced. The unknown curve Γ can be represented by the zero level set of Lipschitz function $\phi: \Omega \rightarrow \mathbb{R}$ such

$$\begin{cases} \Gamma = \partial\Omega_1 = \{(x, y) \in \Omega \mid \phi(x, y) = 0\}, \\ \text{inside}(\Gamma) = \Omega_1 = \{(x, y) \in \Omega \mid \phi(x, y) > 0\}, \\ \text{outside}(\Gamma) = \Omega_2 = \{(x, y) \in \Omega \mid \phi(x, y) < 0\}. \end{cases}$$

Define the Heaviside and the Dirac delta function as

$$H(x) = \begin{cases} 1, & \text{if } x \geq 0, \\ 0, & \text{if } x < 0, \end{cases} \quad \text{and} \quad \delta(x) = H'(x),$$

and given ϕ as above, Eq. (2.2) is rewritten in the following way

$$F(\phi, c_1, c_2) = \mu \int_{\Omega} |\nabla H(\phi)| dx dy + \lambda_1 \int_{\Omega} |z(x, y) - c_1|^2 H(\phi(x, y)) dx dy \\ + \lambda_2 \int_{\Omega} |z(x, y) - c_2|^2 (1 - H(\phi(x, y))) dx dy. \quad (2.3)$$

Once the level set function ϕ is obtained, the segmented image is given by

$$u = c_1 H(\phi) + c_2 (1 - H(\phi)).$$

To minimize F with respect to c_1, c_2 , keeping $\phi(x, y)$ fixed, we have

$$c_1(\phi(x, y)) = \frac{\int_{\Omega} z(x, y) H(\phi(x, y)) dx dy}{\int_{\Omega} H(\phi(x, y)) dx dy}, \quad (2.4)$$

if $\int_{\Omega} H(\phi(x, y)) dx dy > 0$ (i.e., the curve has a nonempty interior in Ω) and

$$c_2(\phi(x, y)) = \frac{\int_{\Omega} z(x, y) (1 - H(\phi(x, y))) dx dy}{\int_{\Omega} (1 - H(\phi(x, y))) dx dy}, \quad (2.5)$$

if $\int_{\Omega} (1 - H(\phi(x, y))) dx > 0$ (i.e., the curve has a nonempty exterior in Ω).

To compute the Euler-Lagrange equation for the unknown function ϕ , as H is not differentiable at the origin, we consider regularized versions of H and δ :

$$H_{\epsilon}(x) = \frac{1}{2} \left(1 + \frac{2}{\pi} \arctan \left(\frac{x}{\epsilon} \right) \right), \quad \delta_{\epsilon}(x) = H'_{\epsilon}(x) = \frac{\epsilon}{\pi(\epsilon^2 + x^2)}, \quad (2.6)$$

where $H_{\epsilon} \rightarrow H$ when $\epsilon \rightarrow 0$. The regularized functional of $F(\phi, c_1, c_2)$ is given by

$$F_{\epsilon}(\phi, c_1, c_2) = \mu \int_{\Omega} \delta_{\epsilon}(\phi(x, y)) |\nabla \phi| dx dy + \lambda_1 \int_{\Omega} |z(x, y) - c_1|^2 H_{\epsilon}(\phi(x, y)) dx dy \\ + \lambda_2 \int_{\Omega} |z(x, y) - c_2|^2 (1 - H_{\epsilon}(\phi(x, y))) dx dy. \quad (2.7)$$

Finally we obtain the following Euler-Lagrange equation for ϕ :

$$\begin{cases} \delta_{\epsilon}(\phi) \left[\mu \nabla \cdot \left(\frac{\nabla \phi}{|\nabla \phi|} \right) - \lambda_1 (z(x, y) - c_1)^2 + \lambda_2 (z(x, y) - c_2)^2 \right] = 0, & \text{in } \Omega, \\ \frac{\delta_{\epsilon}(\phi)}{|\nabla \phi|} \frac{\partial \phi}{\partial \vec{n}} = 0, & \text{on } \partial \Omega, \end{cases} \quad (2.8)$$

where \vec{n} is the unit normal exterior to the boundary $\partial \Omega$, and $\partial \phi / \partial \vec{n}$ is the normal derivative of ϕ at boundary. Then once ϕ is found, the piecewise segmented image is given by $u(x, y) = H_{\epsilon}(\phi(x, y))c_1 + (1 - H_{\epsilon}(\phi(x, y)))c_2$.

2.2 Li-Xu-Gui-Fox model

Improving on the Chan-Vese model, Li-Xu-Gui-Fox [18] proposed a new variational formulation for geometric active contours that forces the level set function to be close to a signed distance function, and therefore completely eliminates the need of the costly re-initialization procedure. Their variational formulation

$$\min_{\phi} \mathcal{E}(\phi) = \mu P(\phi) + \alpha L_g(\phi) + \nu A_g(\phi), \quad (2.9)$$

where $\mu > 0$, $\alpha > 0$ and ν are constants, consists of an internal energy term $\mu P(\phi)$ that penalizes the deviation of the level set function from a signed distance function, and an external energy term $\mathcal{E}_m(\phi) = \alpha L_g(\phi) + \nu A_g(\phi)$ that drives the motion of the zero level set toward the desired image features, such as object boundaries. The terms $P(\phi)$, $L_g(\phi)$ and $A_g(\phi)$ are defined by

$$P(\phi) = \int_{\Omega} \frac{1}{2} (|\nabla\phi| - 1)^2 dx dy, \quad L_g(\phi) = \int_{\Omega} g\delta(\phi) |\nabla\phi| dx dy, \quad A_g(\phi) = \int_{\Omega} gH(-\phi) dx dy,$$

where $g = (1 + |\nabla G_{\sigma} * z(x,y)|^2)^{-1}$ for a given image $z(x,y)$.

By calculus of variations, the Euler-Lagrange equation of (2.9), $\partial\mathcal{E}/\partial\phi = 0$, for the function ϕ is

$$-\mu \left[\Delta\phi - \operatorname{div} \left(\frac{\nabla\phi}{|\nabla\phi|} \right) \right] - \alpha\delta(\phi) \operatorname{div} \left(g \frac{\nabla\phi}{|\nabla\phi|} \right) - \nu g\delta(\phi) = 0, \quad (2.10)$$

where Δ is the Laplacian operator. The steepest descent process for minimization of the functional \mathcal{E} is the following gradient flow:

$$\frac{\partial\phi}{\partial t} = \mu \left[\Delta\phi - \operatorname{div} \left(\frac{\nabla\phi}{|\nabla\phi|} \right) \right] + \alpha\delta(\phi) \operatorname{div} \left(g \frac{\nabla\phi}{|\nabla\phi|} \right) + \nu g\delta(\phi)$$

or

$$\frac{\partial\phi}{\partial t} = \mu \left[\Delta\phi - \operatorname{div} \left(\frac{\nabla\phi}{|\nabla\phi|} \right) \right] + \alpha\delta(\phi) \left[g \operatorname{div} \left(\frac{\nabla\phi}{|\nabla\phi|} \right) + \nabla g \frac{\nabla\phi}{|\nabla\phi|} \right] + \nu g\delta(\phi).$$

Hence the level set evolution can be easily implemented by a finite difference scheme and is computationally efficient.

2.3 Badshah-Chen model

The above models are examples of global segmentation methods. To tackle the task of selective segmentation, these global models are inadequate even if we start an initial contour from within an interested object. Below we review the selective model by Badshah-Chen [4] which is based on the C. Gout and C. Guyader model [14]. Assume that $z(x,y)$ is the given image defined on the rectangular domain Ω .

In a selective segmentation, we hope to detect the features of image z that are defined in a closed domain and to be closest to the geometrical points in a set $A = \{(x_i^*, y_i^*) \in \Omega, 1 \leq i \leq n_1\} \subset \Omega$ consisting of n_1 distinct points near the object boundary to be detected [13,14]. The aim a selective segmentation is to find an optimal contour $\Gamma \subset \Omega$ that represents a closed object and best approaches the points from the set A in some sense of minimal geometric distance.

The C. Gout and C. Guyader model [14] combines the geodesic active contour model [6] with the geometrical constraints of being close to A . An edge detector function g is used, as defined in Eq. (2.11) (other forms can be found in [6, 10, 22])

$$g(w) = \frac{1}{1+w^2}. \quad (2.11)$$

The purpose of the edge detector function g is to stop the evolving curve on edges of the objects in an image. Clearly $g(|\nabla z(x,y)|)$ is zero on edges in an image where w is large and one in flat regions where w is small. A distance function d will be required to stop the evolving curve when approaching the points from set A . Let the function d be defined in the following way [14]:

$$d(x,y) = \text{distance}((x,y), A) = \prod_{i=1}^{n_1} \left[1 - \exp\left(-\frac{(x-x_i^*)^2}{2\tau^2}\right) \exp\left(-\frac{(y-y_i^*)^2}{2\tau^2}\right) \right], \quad \forall (x,y) \in \Omega. \quad (2.12)$$

Another option for d is

$$d(x,y) = \min_{(x_i^*, y_i^*) \in A} |(x,y) - (x_i^*, y_i^*)|$$

as used in [13]. Clearly d acts locally and will be approximately 0 in the neighborhood of points of A . The aim is to find a contour Γ such that $d \simeq 0$ or $g \simeq 0$ along it. They proposed the following model for this purpose

$$\min_{\Gamma} F(\Gamma) = \int_{\Gamma} d(x,y) g(|\nabla z(x,y)|) ds. \quad (2.13)$$

The contour Γ will stop at local minima where $d \simeq 0$ (in the neighborhood of points for A) or $g \simeq 0$ (near object boundaries). When the interested object is not too close to other objects and if the given image z does not have noise, the above model leads to reliable segmentation. In the latter case, using a blurring operator K and replacing $g(|\nabla z(x,y)|)$ by $g(|\nabla Kz(x,y)|)$ to smooth out the noise in z can improve the segmented results but the results are not always satisfactory.

The Badshah-Chen [4] work, improving on (2.13), proposed the following model:

$$\begin{aligned} \min_{\phi(x,y), c_1, c_2} F(\phi(x,y), c_1, c_2) = & \mu \int_{\Omega} d(x,y) g(|\nabla z(x,y)|) |\nabla H(\phi(x,y))| dx dy \\ & + \lambda_1 \int_{\Omega} |z(x,y) - c_1|^2 H(\phi(x,y)) dx dy \\ & + \lambda_2 \int_{\Omega} |z(x,y) - c_2|^2 (1 - H(\phi(x,y))) dx dy, \end{aligned} \quad (2.14)$$

essentially adding two region-based terms

$$\lambda_1 \int_{\text{inside}(\Gamma)} |z(x,y) - c_1|^2 dx dy + \lambda_2 \int_{\text{outside}(\Gamma)} |z(x,y) - c_2|^2 dx dy$$

to (2.13) where H is the Heaviside function.

Since the Heaviside function is not differentiable at the origin, they consider the regularized version of H denoted by H_ϵ and of the corresponding δ by δ_ϵ as with (2.6). Then the minimization problem (2.14) becomes

$$\begin{aligned} \min_{\phi(x,y), c_1, c_2} F_\epsilon(\phi(x,y), c_1, c_2) = & \mu \int_{\Omega} W \delta_\epsilon(\phi(x,y)) |\nabla \phi(x,y)| dx dy \\ & + \lambda_1 \int_{\Omega} |z(x,y) - c_1|^2 H_\epsilon(\phi(x,y)) dx dy \\ & + \lambda_2 \int_{\Omega} |z(x,y) - c_2|^2 (1 - H_\epsilon(\phi(x,y))) dx dy, \end{aligned} \quad (2.15)$$

where $W = d(x,y)g(|\nabla z(x,y)|)$. Keeping $\phi(x,y)$ fixed and minimizing with respect to c_1 and c_2 , one gets the following equations for computing c_1 and c_2

$$c_1(\phi(x,y)) = \frac{\int_{\Omega} z(x,y) H_\epsilon(\phi(x,y)) dx dy}{\int_{\Omega} H_\epsilon(\phi(x,y)) dx dy}, \quad (2.16)$$

if $\int_{\Omega} H_\epsilon(\phi(x,y)) dx dy > 0$ (i.e., if the curve has a nonempty interior in Ω), and

$$c_2(\phi(x,y)) = \frac{\int_{\Omega} z(x,y) (1 - H_\epsilon(\phi(x,y))) dx dy}{\int_{\Omega} (1 - H_\epsilon(\phi(x,y))) dx dy}, \quad (2.17)$$

if $\int_{\Omega} (1 - H_\epsilon(\phi(x,y))) dx dy > 0$ (i.e., if the curve has a nonempty exterior in Ω). Finally keeping c_1 and c_2 fixed, one can minimize (2.15) with respect to $\phi(x,y)$. Thus we have the following Euler-Lagrange equation for ϕ

$$\delta_\epsilon(\phi) \mu \nabla \cdot \left(W \frac{\nabla \phi}{|\nabla \phi|} \right) - \delta_\epsilon(\phi) (\lambda_1 (z(x,y) - c_1)^2 - \lambda_2 (z(x,y) - c_2)^2) = 0, \quad \text{in } \Omega \quad (2.18)$$

with

$$W \frac{\delta_\epsilon(\phi)}{|\nabla \phi|} \frac{\partial \phi}{\partial \vec{n}} = 0, \quad \text{on } \partial \Omega.$$

3 A new variational model

Our new model is motivated by the fact that the region-based terms in (2.14) essentially carry out a global segmentation and new region-based terms are required for local segmentation i.e., selection. To this end, we shall propose a dual level set approach where ϕ_G and ϕ_L are respectively used to carry out global and local segmentation.

For the given image z , we shall use the following notation. Denote by $\Gamma_G = \partial\Omega_G$ in Ω the global evolving curve for locating all features Ω_G of image z . The desired selective curve is denoted by $\Gamma_L = \partial\Omega_L$ in Ω , where we naturally assume Ω_L is contained in Ω_G . Thus we have $\text{inside}(\Gamma_L) = \Omega_L$, $\text{outside}(\Gamma_L) = \Omega \setminus \overline{\Omega_L}$, $\text{inside}(\Gamma_G) = \Omega_G$, $\text{outside}(\Gamma_G) = \Omega \setminus \overline{\Omega_G}$. The two zero level set functions $\phi_L(x,y)$ and $\phi_G(x,y)$ are defined such that

$$\begin{cases} \Gamma_L = \partial\Omega_L = \{(x,y) \in \Omega_L \mid \phi_L(x,y) = 0\}, \\ \text{inside}(\Gamma_L) = \Omega_L = \{(x,y) \in \Omega_L \mid \phi_L(x,y) > 0\}, \\ \text{outside}(\Gamma_L) = \Omega \setminus \overline{\Omega_L} = \{(x,y) \in \Omega_L \mid \phi_L(x,y) < 0\}, \\ \Gamma_G = \partial\Omega_G = \{(x,y) \in \Omega \mid \phi_G(x,y) = 0\}, \\ \text{inside}(\Gamma_G) = \Omega_G = \{(x,y) \in \Omega \mid \phi_G(x,y) > 0\}, \\ \text{outside}(\Gamma_G) = \Omega \setminus \overline{\Omega_G} = \{(x,y) \in \Omega \mid \phi_G(x,y) < 0\}. \end{cases}$$

In this way we replace the unknown quantities Γ_L by ϕ_L and Γ_G by ϕ_G shortly. To explore possible advantages of having an enlarged domain of Ω_G within a distance of γ away, we define

$$\Omega_{G,\gamma} = \{(x,y) \in \Omega \mid \phi_G(x,y) > -\gamma\},$$

where the parameter $\gamma \geq 0$ will be taken as 0 or 3. Note $\Omega_L \subset \Omega_G \subseteq \Omega_{G,\gamma} \subset \Omega$.

Then realizing the idea of looking all features Ω_G in the whole image domain Ω and the selective features Ω_L in the local domain Ω_G , our new variational model is the following

$$\begin{aligned} & \min_{\Gamma_L, \Gamma_G, c_1, c_2} F(\Gamma_L, \Gamma_G, c_1, c_2) \\ &= \mu_1 \int_{\Gamma_L} d(x,y) g(|\nabla z(x,y)|) ds + \mu_2 \int_{\Gamma_G} g(|\nabla z(x,y)|) ds \\ & \quad + \lambda_{1G} \int_{\text{inside}(\Gamma_G)} |z(x,y) - c_1|^2 dx dy + \lambda_{2G} \int_{\text{outside}(\Gamma_G)} |z(x,y) - c_2|^2 dx dy \\ & \quad + \lambda_1 \int_{\text{inside}(\Gamma_L)} |z(x,y) - c_1|^2 dx dy + \lambda_2 \int_{\text{outside}(\Gamma_L) \cap \text{inside}(\Gamma_G)} |z(x,y) - c_1|^2 dx dy \\ & \quad + \lambda_3 \int_{\text{outside}(\Gamma_L) \cap \text{outside}(\Gamma_G)} |z(x,y) - c_2|^2 dx dy, \end{aligned} \tag{3.1}$$

where

$$g(|\nabla z(x,y)|) = \frac{1}{1 + |\nabla G_\sigma(x,y) * z(x,y)|^2}, \tag{3.2}$$

parameters $\mu_1, \mu_2, \lambda_{1G}, \lambda_{2G}, \lambda_1, \lambda_2, \lambda_3$ are all positive, $d(x,y)$ is a distance function from the given geometric markers in set A as defined in [4]. Here $G_\sigma(x,y) * z(x,y)$ as a smooth version of $z(x,y)$ with Gaussian $G_\sigma(x,y) = \sigma^{-1/2} e^{-|x^2+y^2|/4\sigma}$ is to deal with possible noise (in our experiments for the image with strong noise, $\sigma = 1/2$ is taken).

When deriving level set formulation for (3.1), we make these two decisions. Firstly both level set functions $\phi_L(x,y), \phi_G(x,y)$ will be automatically scaled with new terms

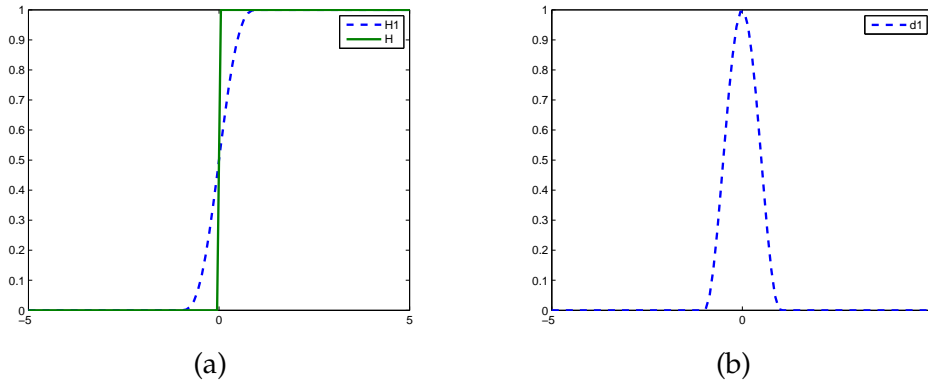


Figure 3: (a) The Heaviside function H and the approximation H_ϵ (b) function δ_ϵ .

similar to $P(\phi)$ in (2.9) to avoid re-initialization. Secondly we like to constrain the search domain for computing the weighted length of Γ_L to $\Omega_{G,\gamma}$ instead of Ω since

$$\begin{aligned} \int_{\Gamma_L} d(x,y)g(|\nabla z(x,y)|)ds &= \int_{\Omega} d(x,y)g(|\nabla z(x,y)|)|\nabla H(\phi_L(x,y))|dxdy \\ &= \int_{\Omega_{G,\gamma}} d(x,y)g(|\nabla z(x,y)|)|\nabla H(\phi_L(x,y))|dxdy \\ &= \int_{\Omega} d(x,y)g(|\nabla z(x,y)|)|\nabla H(\phi_L(x,y))|H(\phi_G(x,y)+\gamma)dxdy. \end{aligned}$$

We shall follow the same procedure of treating the non-differentiable H function by replacing it with H_ϵ a regularized Heaviside function as in [3, 9]. Fig. 3 shows a regularized Heaviside function (H_1 compared to H) and its derivative. Different regularized Heaviside functions can be used e.g.,

$$H_{1\epsilon} = \begin{cases} 0, & z < -\epsilon, \\ \frac{1}{2} \left[1 + \frac{z}{\epsilon} + \frac{1}{\pi} \sin\left(\frac{\pi z}{\epsilon}\right) \right], & |z| \leq \epsilon, \\ 1, & z > \epsilon, \end{cases}$$

$$H_{2\epsilon} = \frac{1}{2} \left(1 + \operatorname{erf}\left(\frac{\epsilon}{z}\right) \right), \quad H_{3\epsilon} = \frac{1}{2} \left(1 + \frac{2}{\pi} \arctan\left(\frac{z}{\epsilon}\right) \right).$$

The error function $\operatorname{erf}(x)$ is twice the integral of the Gaussian distribution with 0 mean and variance of 1/2 in the form

$$\operatorname{erf}(x) = \frac{2}{\sqrt{\pi}} \int_0^x e^{-t^2} dt.$$

The differences between $H_{1\epsilon}, H_{2\epsilon}$ and $H_{3\epsilon}$ and their corresponding delta function $\delta_{1\epsilon}, \delta_{2\epsilon}$ and $\delta_{3\epsilon}$ are that the first two functions have a small support in the interval $[-\epsilon, \epsilon]$, while

$H_{3\epsilon}$ and its corresponding $\delta_{3\epsilon}$ are different from zero everywhere. The above observation suggests that $H_{3\epsilon}$ may not be suitable for the extreme case where the interested feature is less than 2 pixels away from other features; adjusting ϵ will resolve the problem but we lose the automatic capability. So our suggestion is to use $H_{1\epsilon}$, or $H_{2\epsilon}$ while we may use $H_{3\epsilon}$ for less challenging problems.

With a regularized Heaviside, the Eq. (3.1) can be rewritten as

$$\begin{aligned} & \min_{\phi_L(x,y), \phi_G(x,y), c_1, c_2} F_\epsilon(\phi_L(x,y), \phi_G(x,y), c_1, c_2) \\ = & \mu_1 \int_{\Omega} d(x,y) g(|\nabla z(x,y)|) \delta_\epsilon(\phi_L(x,y)) |\nabla \phi_L(x,y)| H_\epsilon(\phi_G(x,y) + \gamma) dx dy \\ & + \frac{\mu_L}{2} \int_{\Omega} (|\nabla \phi_L(x,y)| - 1)^2 dx dy + \mu_2 \int_{\Omega} g(|\nabla z(x,y)|) \delta_\epsilon(\phi_G(x,y)) |\nabla \phi_G(x,y)| dx dy \\ & + \frac{\mu_G}{2} \int_{\Omega} (|\nabla \phi_G(x,y)| - 1)^2 dx dy + \lambda_{1G} \int_{\Omega} |z(x,y) - c_1|^2 H_\epsilon(\phi_G(x,y)) dx dy \\ & + \lambda_{2G} \int_{\Omega} |z(x,y) - c_2|^2 (1 - H_\epsilon(\phi_G(x,y))) dx dy + \lambda_1 \int_{\Omega} |z(x,y) - c_1|^2 H_\epsilon(\phi_L(x,y)) dx dy \\ & + \lambda_2 \int_{\Omega} |z(x,y) - c_1|^2 (1 - H_\epsilon(\phi_L(x,y))) H(\phi_G(x,y)) dx dy \\ & + \lambda_3 \int_{\Omega} |z(x,y) - c_2|^2 (1 - H_\epsilon(\phi_L(x,y))) (1 - H_\epsilon(\phi_G(x,y))) dx dy. \end{aligned} \tag{3.3}$$

Here μ_L, μ_G are positive. For brevity, we use d, z, ϕ_L, ϕ_G to denote $d(x,y), z(x,y), \phi_L(x,y)$ and $\phi_G(x,y)$. Keeping ϕ fixed and minimizing with respect to c_1 and c_2 , we have the following equations for computing c_1 and c_2 :

$$c_1 = \frac{\lambda_{1G} \int_{\Omega} z H_\epsilon(\phi_G) dx dy + \lambda_1 \int_{\Omega} z H_\epsilon(\phi_L) dx dy + \lambda_2 \int_{\Omega} z (1 - H_\epsilon(\phi_L)) H_\epsilon(\phi_G) dx dy}{\lambda_{1G} \int_{\Omega} H_\epsilon(\phi_G) dx dy + \lambda_1 \int_{\Omega} H_\epsilon(\phi_L) dx dy + \lambda_2 \int_{\Omega} (1 - H_\epsilon(\phi_L)) H_\epsilon(\phi_G) dx dy}, \tag{3.4a}$$

$$c_2 = \frac{\lambda_{2G} \int_{\Omega} z (1 - H_\epsilon(\phi_G)) dx dy + \lambda_3 \int_{\Omega} z (1 - H_\epsilon(\phi_L)) (1 - H_\epsilon(\phi_G)) dx dy}{\lambda_{2G} \int_{\Omega} (1 - H_\epsilon(\phi_G)) dx dy + \lambda_3 \int_{\Omega} (1 - H_\epsilon(\phi_L)) (1 - H_\epsilon(\phi_G)) dx dy}, \tag{3.4b}$$

if we assume the $\phi_G(x,y)$ has neither empty interior nor empty exterior.

Now keeping c_1 and c_2 fixed, we minimize (3.3) with respect to $\phi_L(x,y)$ and $\phi_G(x,y)$. We first minimize F_ϵ with respect to ϕ_L by using the Gâteaux derivatives to find the first variation of the functional F_ϵ with respect to ϕ_L

$$\lim_{h \rightarrow 0} \frac{d}{dh} (F_\epsilon(\phi_L + h\psi, c_1, c_2)) = 0.$$

Using the same W as in (2.15), the following Euler-Lagrange equation for ϕ_L can be de-

rived:

$$\left\{ \begin{array}{l} \mu_1 \delta_\epsilon(\phi_L) \nabla \cdot \left(WH_\epsilon(\phi_G + \gamma) \frac{\nabla \phi_L}{|\nabla \phi_L|} \right) + \mu_L \nabla \cdot \left(\left(1 - \frac{1}{|\nabla \phi_L|} \right) \nabla \phi_L \right) \\ \quad + \delta_\epsilon(\phi_L) (-\lambda_1(z(x,y) - c_1)^2 + \lambda_2(z(x,y) - c_1)^2 H_\epsilon(\phi_G)) \\ \quad + \lambda_3(z(x,y) - c_2)^2 (1 - H_\epsilon(\phi_G))) = 0, \\ \frac{\partial \phi_L}{\partial \vec{n}} = 0, \end{array} \right. \quad \begin{array}{l} \text{in } \Omega, \\ \text{on } \partial\Omega, \end{array} \quad (3.5)$$

where boundary conditions

$$\mu_1 WH_\epsilon(\phi_G + \gamma) \frac{\delta_\epsilon(\phi_L)}{|\nabla \phi_L|} \frac{\partial \phi_L}{\partial \vec{n}} = 0 \quad \text{and} \quad \mu_L (|\phi_L| - 1) \frac{1}{|\nabla \phi_L|} \frac{\partial \phi_L}{\partial \vec{n}} = 0$$

reduce to Neumann boundary condition. In the same way we may derive the Euler-Lagrange equation for ϕ_G .

In equations for ϕ_G and ϕ_L , balloon terms such as $\alpha W |\nabla \phi_L|$, $\alpha g(x,y) |\nabla \phi_G|$ respectively can be added to speed up the convergence. The final equations of ϕ_G and ϕ_L can be written in the form

$$\left\{ \begin{array}{l} \mu_1 \delta_\epsilon(\phi_L) \nabla \cdot \left(WH_\epsilon(\phi_G + \gamma) \frac{\nabla \phi_L}{|\nabla \phi_L|} \right) + \mu_L \nabla \cdot \left(\left(1 - \frac{1}{|\nabla \phi_L|} \right) \nabla \phi_L \right) \\ \quad + \delta_\epsilon(\phi_L) (-\lambda_1(z(x,y) - c_1)^2 + \lambda_2(z(x,y) - c_1)^2 H_\epsilon(\phi_G)) \\ \quad + \lambda_3(z(x,y) - c_2)^2 (1 - H_\epsilon(\phi_G))) + \alpha W(x,y) |\nabla \phi_L| = 0, \\ \frac{\partial \phi_L}{\partial \vec{n}} = 0, \end{array} \right. \quad \begin{array}{l} \text{in } \Omega, \\ \text{on } \partial\Omega, \end{array} \quad (3.6)$$

and

$$\left\{ \begin{array}{l} \mu_2 \delta_\epsilon(\phi_G) \nabla \cdot \left(g(x,y) \frac{\nabla \phi_G}{|\nabla \phi_G|} \right) + \mu_G \nabla \cdot \left(\left(1 - \frac{1}{|\nabla \phi_G|} \right) \nabla \phi_G \right) \\ \quad + \delta_\epsilon(\phi_G + \gamma) (-\mu_1 W(x,y) |\nabla H_\epsilon(\phi_L)|) + \delta_\epsilon(\phi_G) (-\lambda_{1G}(z(x,y) - c_1)^2 \\ \quad + \lambda_{2G}(z(x,y) - c_2)^2 - \lambda_2(z(x,y) - c_1)^2 (1 - H(\phi_L))) \\ \quad + \lambda_3(z(x,y) - c_2)^2 (1 - H(\phi_L)) + \alpha g(x,y) |\nabla \phi_G| = 0, \\ \frac{\partial \phi_G}{\partial \vec{n}} = 0, \end{array} \right. \quad \begin{array}{l} \text{in } \Omega, \\ \text{on } \partial\Omega. \end{array} \quad (3.7)$$

By freezing the nonlinear coefficients in Eqs. (3.6) and (3.7) we get linearised systems of equations which can be solved by a fixed point method. Since the drawback of this method is the computational cost of the associated linear system for large image, we develop a fast method similar to [4, 14, 33, 34].

4 An additive operator splitting algorithm

In order to develop an additive operator splitting (AOS) method [20, 34] for (3.6) and (3.7), we consider the following related parabolic equations:

$$\left\{ \begin{array}{l} \phi_L(x,y,0) = \phi_L^0(x,y), \\ \frac{\partial \phi_L}{\partial t} = \mu_1 \delta_\epsilon(\phi_L) \nabla \cdot \left(WH_\epsilon(\phi_G + \gamma) \frac{\nabla \phi_L}{|\nabla \phi_L|} \right) + \mu_L \nabla \cdot \left(\left(1 - \frac{1}{|\nabla \phi_L|} \right) \nabla \phi_L \right) \\ \quad + \delta_\epsilon(\phi_L) (-\lambda_1(z(x,y) - c_1)^2 + \lambda_2(z(x,y) - c_1)^2 H_\epsilon(\phi_G) \\ \quad + \lambda_3(z(x,y) - c_2)^2 (1 - H_\epsilon(\phi_G))) + \alpha W(x,y) |\nabla \phi_L|, \\ \frac{\partial \phi_L}{\partial \vec{n}} \Big|_{\partial \Omega} = 0, \end{array} \right. \tag{4.1a}$$

$$\left\{ \begin{array}{l} \phi_G(x,y,0) = \phi_G^0(x,y) \\ \frac{\partial \phi_G}{\partial t} = \mu_2 \delta_\epsilon(\phi_G) \nabla \cdot \left(g(x,y) \frac{\nabla \phi_G}{|\nabla \phi_G|} \right) + \mu_G \nabla \cdot \left(\left(1 - \frac{1}{|\nabla \phi_G|} \right) \nabla \phi_G \right) \\ \quad + \delta_\epsilon(\phi_G + \gamma) (-\mu_1 W(x,y) | \nabla H_\epsilon(\phi_L) |) + \alpha g(x,y) |\nabla \phi_G| \\ \quad + \delta_\epsilon(\phi_G) (-\lambda_{1G}(z(x,y) - c_1)^2 + \lambda_{2G}(z(x,y) - c_2)^2 \\ \quad - \lambda_2(z(x,y) - c_1)^2 (1 - H(\phi_L)) + \lambda_3(z(x,y) - c_2)^2 (1 - H(\phi_L))), \\ \frac{\partial \phi_G}{\partial \vec{n}} \Big|_{\partial \Omega} = 0. \end{array} \right. \tag{4.1b}$$

By denoting

$$\begin{aligned} f_L &= \delta_\epsilon(\phi_L) (-\lambda_1(z(x,y) - c_1)^2 + \lambda_2(z(x,y) - c_1)^2 H_\epsilon(\phi_G) \\ &\quad + \lambda_3(z(x,y) - c_2)^2 (1 - H_\epsilon(\phi_G))) + \alpha W(x,y) |\nabla \phi_L|, \\ f_G &= \delta_\epsilon(\phi_G + \gamma) (-\mu_1 W(x,y) H_\epsilon(\phi_L)) + \delta_\epsilon(\phi_G) (-\lambda_{1G}(z(x,y) - c_1)^2 + \lambda_{2G}(z(x,y) - c_2)^2 \\ &\quad - \lambda_2(z(x,y) - c_1)^2 (1 - H(\phi_L)) + \lambda_3(z(x,y) - c_2)^2 (1 - H(\phi_L))) + \alpha g(x,y) |\nabla \phi_G|, \\ F_L &= \frac{WH_\epsilon(\phi_G + \gamma)}{|\nabla \phi_L|}, \quad F_G = \frac{g}{|\nabla \phi_G|}, \quad E_L = 1 - \frac{1}{|\nabla \phi_L|}, \quad E_G = 1 - \frac{1}{|\nabla \phi_G|}, \end{aligned}$$

Eqs. (4.1b) and (4.1a) can be written in the compact form:

$$\left\{ \begin{array}{l} \frac{\partial \phi_L}{\partial t} = \mu_1 \delta_\epsilon(\phi_L) \nabla \cdot (F_L \nabla \phi_L) + \mu_L \nabla \cdot (E_L \nabla \phi_L) + f_L \\ \quad = \mu_1 \delta_\epsilon(\phi_L) (\partial_x (F_L \partial_x \phi_L) + \partial_y (F_L \partial_y \phi_L)) + \mu_L (\partial_x (E_L \partial_x \phi_L) + \partial_y (E_L \partial_y \phi_L)) + f_L, \\ \frac{\partial \phi_G}{\partial t} = \mu_2 \delta_\epsilon(\phi_G) \nabla \cdot (F_G \nabla \phi_G) + \mu_G \nabla \cdot (E_G \nabla \phi_G) + f_G \\ \quad = \mu_2 \delta_\epsilon(\phi_G) (\partial_x (F_G \partial_x \phi_G) + \partial_y (F_G \partial_y \phi_G)) + \mu_G (\partial_x (E_G \partial_x \phi_G) + \partial_y (E_G \partial_y \phi_G)) + f_G. \end{array} \right. \tag{4.2}$$

Since the coefficients contain the nonlinearities, and ϕ_G, ϕ_L depend on each other, we have to iterate the above equations. Note that both equations in (4.2) are of similar self-adjoint

form. It suffices to consider how to solve the second equation:

$$\frac{\partial \phi_G}{\partial t} = \mu_2 \delta_\epsilon(\phi_G) (\partial_x (F_G \partial_x \phi_G) + \partial_y (F_G \partial_y \phi_G)) + \mu_G (\partial_x (E_G \partial_x \phi_G) + \partial_y (E_G \partial_y \phi_G)) + f_G. \quad (4.3)$$

Below we shall write ϕ, F, E after dropping the subscripts in ϕ_G, F_G, E_G .

Discretizing with spatial step size $h_1 = h_2 = h = 1$, the Eq. (4.3) leads to the semi-implicit equation in x -coordinate direction

$$\begin{aligned} \frac{\phi_{i,j}^{k+1} - \phi_{i,j}^k}{2\Delta t} &= \mu_2 \delta_\epsilon(\phi_i) \left(\left(\frac{F_{i,j}^k + F_{i+1,j}^k}{2h^2} \right) (\phi_{i+1,j}^{k+1} - \phi_{i,j}^{k+1}) - \left(\frac{F_{i,j}^k + F_{i-1,j}^k}{2h^2} \right) (\phi_{i,j}^{k+1} - \phi_{i-1,j}^{k+1}) \right) \\ &\quad + \mu_G \left(\left(\frac{E_{i,j}^k + E_{i+1,j}^k}{2h^2} \right) (\phi_{i+1,j}^{k+1} - \phi_{i,j}^{k+1}) - \left(\frac{E_{i,j}^k + E_{i-1,j}^k}{2h^2} \right) (\phi_{i,j}^{k+1} - \phi_{i-1,j}^{k+1}) \right) + \frac{1}{2} f_{i,j}, \end{aligned} \quad (4.4)$$

$$\Rightarrow \phi_{i,j}^{k+1} = \phi_{i,j}^k + 2\Delta t (w_1 \phi_{i+1,j}^{k+1} - w_2 \phi_{i,j}^{k+1} + w_3 \phi_{i-1,j}^{k+1}) + \Delta t f_{i,j}, \quad (4.5)$$

where

$$w_1 = \mu_2 \delta_\epsilon(\phi_{i,j}) \frac{F_{i,j}^k + F_{i+1,j}^k}{2h^2} + \mu_G \frac{E_{i,j}^k + E_{i+1,j}^k}{2h^2}, \quad (4.6a)$$

$$w_2 = \mu_2 \delta_\epsilon(\phi_{i,j}) \frac{F_{i-1,j}^k + 2F_{i,j}^k + F_{i+1,j}^k}{2h^2} + \mu_G \frac{E_{i-1,j}^k + 2E_{i,j}^k + E_{i+1,j}^k}{2h^2}, \quad (4.6b)$$

$$w_3 = \mu_2 \delta_\epsilon(\phi_{i,j}) \frac{F_{i,j}^k + F_{i-1,j}^k}{2h^2} + \mu_G \frac{E_{i,j}^k + E_{i-1,j}^k}{2h^2}. \quad (4.6c)$$

Similarly, in y -coordinate direction, one gets

$$\Rightarrow \phi_{i,j}^{k+1} = \phi_{i,j}^k + 2\Delta t (\bar{w}_1 \phi_{i,j+1}^{k+1} - \bar{w}_2 \phi_{i,j}^{k+1} + \bar{w}_3 \phi_{i,j-1}^{k+1}) + \Delta t f_{i,j}. \quad (4.7)$$

In the spirit of AOS, we solve the decoupled system of Eqs. (4.5) and (4.7) with time step $2\Delta t$ respectively in the x, y -direction and then average the two solutions with the result equivalent to solving a coupled semi-implicit system with the time step Δt . In matrix notation, Eqs. (4.5) and (4.7) can be written as:

$$(I - 2\Delta t A_l(\phi^k)) \phi_l^{k+1} = \hat{f}^k, \quad \text{for } l=1,2: \quad \phi^{k+1} = \frac{1}{2} \sum_{l=1}^2 \phi_l^{k+1}, \quad k=0,1,\dots,$$

where $\hat{f}^k = \phi^k + \Delta t f^k$, I is the identity matrix and A_l is a tridiagonal matrix respectively for $l=1,2$ consisting of $\{w_1, -w_2, w_3\}$ and $\{\bar{w}_1, -\bar{w}_2, \bar{w}_3\}$ (adjusted at boundary nodes).

5 Experimental results

In order to illustrate the robustness of our proposed model we present further numerical results from segmentation of a range of artificial, synthetic and real images, with different

types of contours and shapes. We also compare our work with Badshah-Chen [4]; as we shall see, for problems which can be solved by both models, our method is less dependent on the choice of regularized Heaviside functions used while there exist some cases where the latter method does not work.

In our numerical experiments, we generally choose two image sizes $n = 128, 256$ and the parameters as follows:

$$\begin{aligned} \lambda_{1G} &= 1, \quad \lambda_{2G} = 1, \quad \lambda_1 = 1, \quad \lambda_2 = 1, \quad \lambda_3 = 1, \quad \tau = 4, \quad h = 1 \quad (\text{the step space}), \\ \Delta t &= 0.1 \quad \text{or} \quad 0.01 \quad (\text{the time step}), \quad \alpha = 0.001, \\ \mu_L &= 0.4, \quad \mu_G = 0.4, \quad \mu_1 = n^2/10, \quad \mu_2 = n^2/10 \end{aligned}$$

(if a given image has no noise, then all μ parameters can be chosen smaller). The initial global level set, placed as a circle, has the form

$$\phi_G^0 = \sqrt{(x - x_G^0)^2 + (y - y_G^0)^2} - r_G^0$$

(where (x_G^0, y_G^0) is the center of the circle, usually at the center of Ω and $r_G^0 = n/5$ the radius), and the initial local level set is placed similarly as

$$\phi_L^0 = \sqrt{(x - x_L^0)^2 + (y - y_L^0)^2} - r_L^0,$$

where (x_L^0, y_L^0) is the center of the markers in set A and the radius r_L^0 is the minimum distance of the markers $r_L^0 = \min_{a \neq b} \|p_a - p_b\|$, where $p_a, p_b \in A$; here

$$x_L^0 = \frac{\sum x\text{-comp of markers}}{\text{no. of markers}}, \quad y_L^0 = \frac{\sum y\text{-comp of markers}}{\text{no. of markers}}.$$

Since $H_{1\epsilon}$ and $H_{2\epsilon}$ lead to spurious results, in our experiments we try approximations $H_{1\epsilon}$, $H_{3\epsilon}$ and corresponding $\delta_{1\epsilon}$ and $\delta_{3\epsilon}$ with $\epsilon = h = 1$; note $H_{3\epsilon}$ has a bigger support in the interval $[-\epsilon, \epsilon]$, which means that with it a moderately large ϵ may lead to spurious results.

In test comparisons, the initial local level set initialization and the choices of parameters are the same for the Badshah-Chen method [4].

5.1 Test Set 1 – robustness of the new model

First we show some numerical results of our new method for segmenting 8 different images. The top left image in Fig. 4 shows an image with many features where the spiral was the aim of detection. The top right image shows results of all features captured by our global level set, and the last images show the segmentation result of the spiral using 3 geometric markers.

In Fig. 5, we test the model on a real CT image where the right kidney is to be selected; again the bottom two images show the correctly segmented organ, using 3 geometric markers.

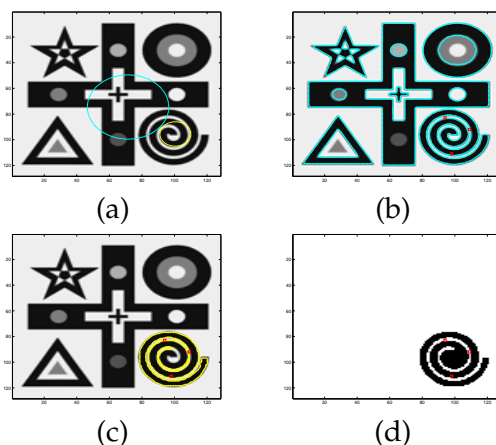


Figure 4: Problem 1 of Test Set 1 by the new model — Successful detection of the spiral in a clean and synthetic image with 3 markers. (a) Initial zero level set contours with $dt=0.1$ ($n=128$); (b) Successful global segmentation by the New model; (c-d) Successful local segmentation and the segmented feature. CPU time=56.3.

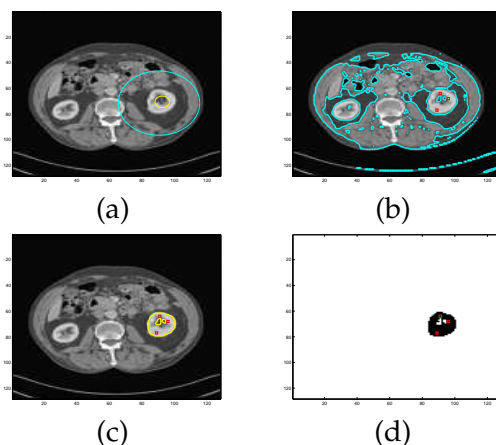


Figure 5: Problem 2 of Test Set 1 by the new model — Successful detection of the right kidney in a real CT image with 3 markers. (a) Initial zero level set contours with $dt=0.01$ ($n=128$); (b) Successful global segmentation by the New model; (c-d) Successful local segmentation and the segmented feature. CPU time=69.1.

Fig. 6 shows three test results (of an artificial flower, the cameraman and a cell image) by our model; clearly our selection model delivers good results.

Finally Fig. 7 shows three more results obtained from segmentation of images with strong noise or smooth contours. Again our model gives the correctly segmented results satisfying the expected selection requirement.

5.2 Test Set 2 – comparison of segmentation of easier problems

As far as selective segmentation is concerned, easier problems refer to those images where the selective target is well separated from all other nearby features; in the ex-

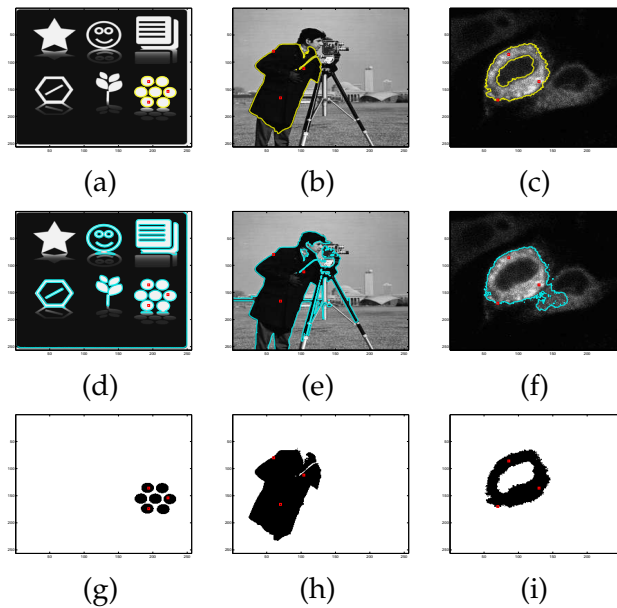


Figure 6: Problems 3-5 of Test Set 1 by the new model — (a) Successful detection of the flower in a clean and synthetic image with 3 markers; (b) cameraman in a clean and real image with 3 markers; (c) one cell in a real image with 3 markers. Here we take $dt = 0.1$ ($n = 256$). The first row shows the selected object from using 3 markers, the second row the final global level set selection and the third row the selected feature. CPU time = 120.4, 138.2 and 517.8 respectively.

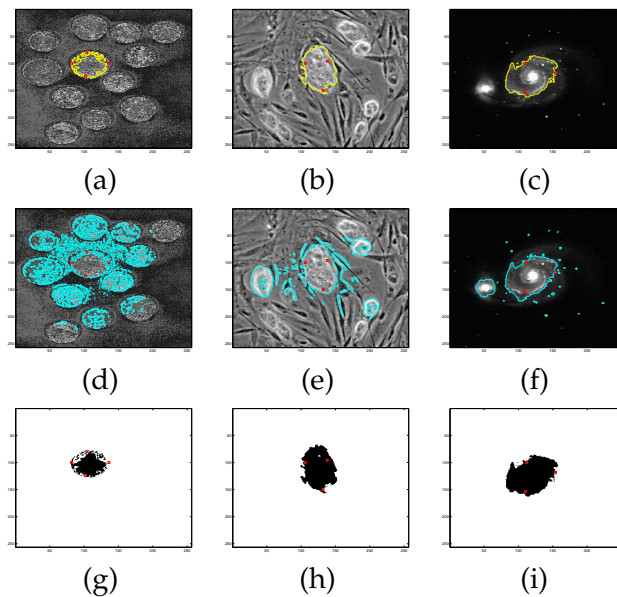


Figure 7: Problems 6-8 of Test Set 1 by the new model — (a) Successful detection of one coin in a strong noise image with 3 markers; (b) one cell in a real image of mouse embryonic stem cells with 3 markers; (c) selection of the main galaxy with 3 markers. Here we take $dt = 0.01$ ($n = 256$). The first row shows the selected object from using 3 markers, the second row the final global level set selection and the third row the selected feature. CPU time = 221.2, 885.0 and 183.3 respectively.

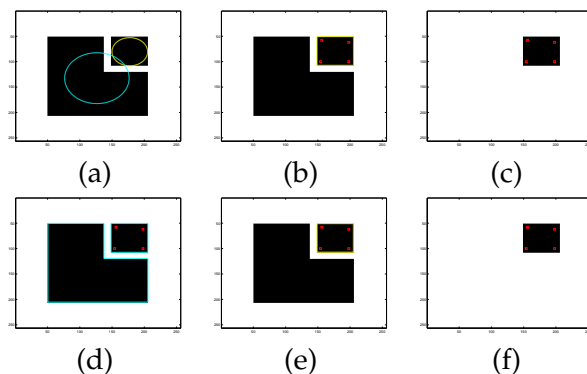


Figure 8: Problem 1 in Test Set 2: Identical results by [4] (top row) and this model (bottom row). (a) Initial zero level set contours with $dt=0.01$ ($n=256$); CPU time=48.5; (d) Successful global segmentation by the New model; (e-f) Successful local segmentation of the box with 4 markers by the New model, with CPU time=117.6.

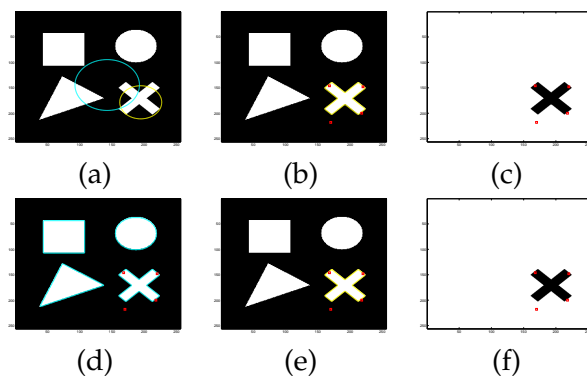


Figure 9: Problem 2 in Test Set 2: Identical results by [4] (top row) and this model (bottom row). (a) Initial zero level set contours with $dt=0.1$ ($n=256$); (b-c) Successful result and the selected feature with [4], with CPU time=50.7; (d) Successful global segmentation by the New model; (e-f) Successful local segmentation of the cross with 4 markers by the New model, with CPU time=118.8.

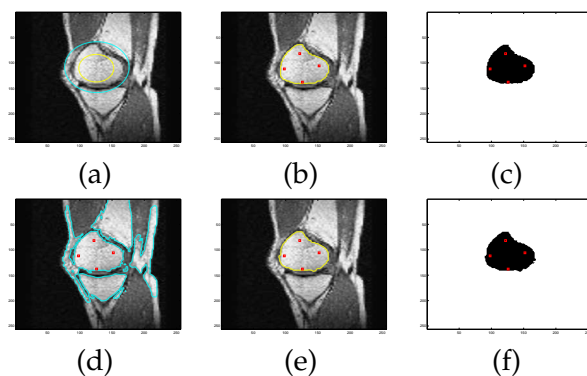


Figure 10: Problem 3 in Test Set 2: Identical results by [4] (top row) and this model (bottom row). (a) Initial zero level set contours with $dt=0.1$ ($n=256$); (b-c) Successful result and the selected feature with [4], with CPU time=62.7; (d) Successful global segmentation by the New model; (e-f) Successful local segmentation of the knee cap with 4 markers by the New model, with CPU time=142.3.

trreme case where the separation distance is extremely large and the target feature is of a simple convex shape, one may even use the non-segmentation models such as [11, 18] by starting evolving contours near the geometric markers. Practically the above distance of more than 3 pixels away may lead to an easy problem.

We now compare our model with Badshah-Chen [4] for three easier problems as shown in Figs. 8, 9, 10; comparative results between [4] and [13, 14] can be found in [4]. For the test results in Fig. 10, although both models give required and almost identical segmentation from using $H_{1\epsilon}$ or $H_{2\epsilon}$, the Badshah-Chen method is more sensitive to the ϵ parameter choice for the regularized Heaviside $H_{3\epsilon}$; specifically our model would work for $\epsilon = 0.01$, or $\epsilon = 1$ while the Badshah-Chen method must use the smaller parameter (otherwise redundant features are captured).

5.3 Test Set 3 – comparison of segmentation of harder problems

Our final set of 4 test problems are harder and more challenging due to a small separation distance between features and a small intensity difference between features and background. In these difficult cases, the previous models from [4, 13, 14] will not work. Figs. 11, 12, 13 and 14 show four respective images and their segmented results of one feature; in each case, the top line of images shows the results of [4] which are not correct due to inclusion of redundant features in the selective segmentation and the bottom line shows the correctly segmented results by our new model. Clearly our model is robust. Here we used the third regularized Heaviside $H_{3\epsilon}$ with $\epsilon = 1$.

5.4 Test Set 4 – necessity of a selection model

Here we show one final experiment to reiterate on the importance of a selective segmentation model in clear contrast to other widely known methods for global segmentation.

In Fig. 15, we compare three sets of usual segmentation results with our selective segmentation result. Here the image in Fig. 15(a) is the original image, given with the markers indicating where the feature is to be extracted. First (a) is segmented by the Chan-Vese [11] algorithm to obtain the segmented image in Fig. 15(b). Then two cropped and smaller images (c)-(d) of Fig. 15(a) are respectively segmented to give the results in (e)-(f). Finally our proposed method gives the correctly segmented result in Fig. 15(g)-(h).

Clearly one observes that only a selective model such as ours can deliver the required and correct segmentation in such situations where selection is needed.

6 Conclusions

Selective image segmentation is an important and practical problem in image processing, where only certain image features defined by geometric constraints are desired. In this paper we presented a new variational model with two level set functions (one for global

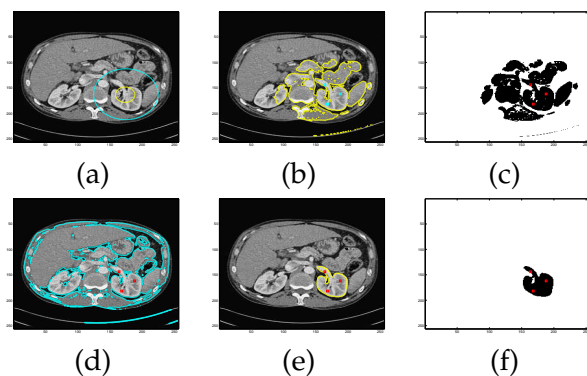


Figure 11: Test Set 3 — Comparative results for Problem 1: (a) Initial zero level set contours with $dt=0.1$ ($n=256$); (b) Unsuccessful result by [4] model; (c) Redundant features selected with [4]; (d) Successful global segmentation by the New model; (e-f) Successful local segmentation of the right kidney with 3 markers with the New model, CPU time=173.1.

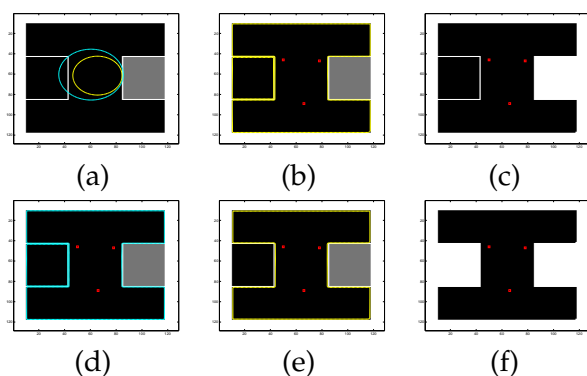


Figure 12: Test Set 3 — Comparative results for Problem 2: (a) Initial zero level set contours with $dt=0.01$ ($n=128$); (b) Unsuccessful result by [4] model; (c) Redundant shapes selected with [4]; (d) Successful global segmentation by the New model; (e-f) Successful local segmentation of a non-convex shape with 3 markers with the New model, CPU time=49.2.

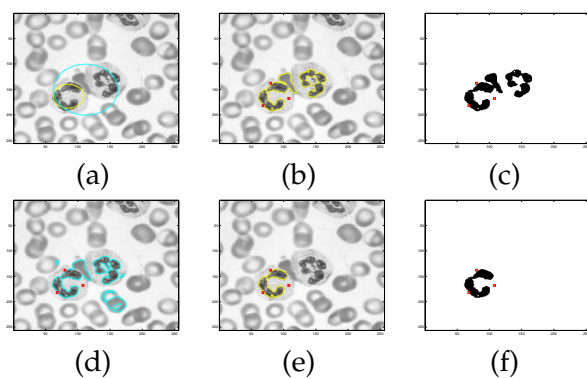


Figure 13: Test Set 3 — Comparative results for Problem 3: (a) Initial zero level set contours with $dt=0.01$ ($n=256$); (b) Unsuccessful result by [4] model; (c) Redundant cells selected with [4]; (d) Successful global segmentation by the New model; (e-f) Successful local segmentation of a single cell with 3 markers with the New model, with CPU time=217.1.

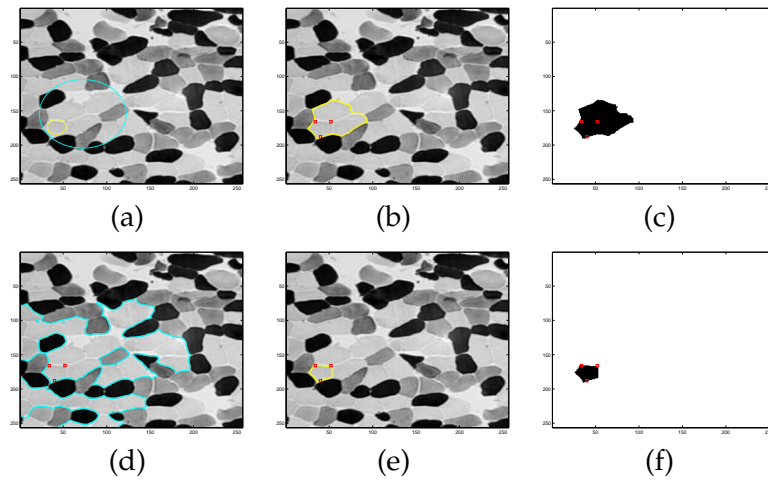


Figure 14: Test Set 3 — Comparative results for Problem 4: (a) Initial zero level set contours with $dt=0.01$ ($n=256$); (b) Unsuccessful result by [4] model; (c) Redundant cells selected with [4]; (d) Successful global segmentation by the New model; (e-f) Successful local segmentation of a cell with 3 markers with the New model, with CPU time=178.1.

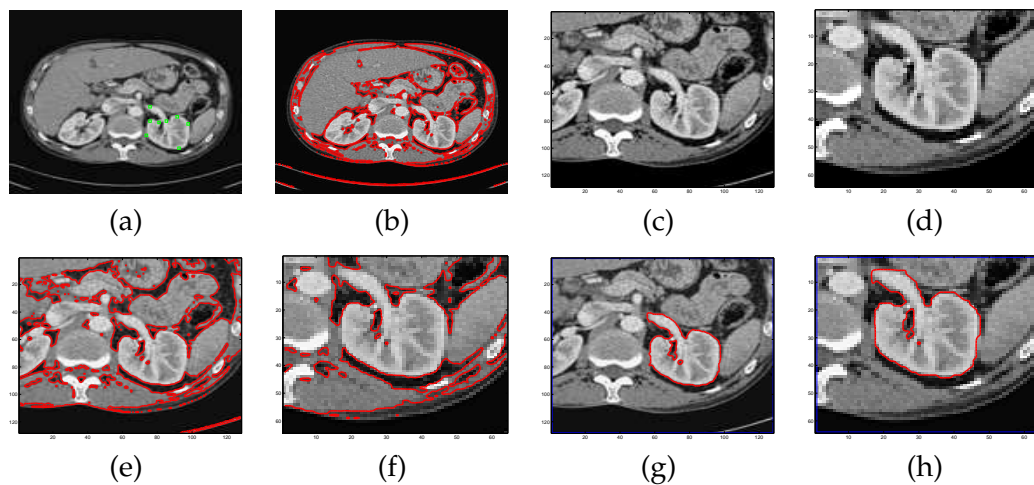


Figure 15: Test Set 4 — Comparative results for Problem 4: (a) Given image with the markers set ($n=256$); (b) Result by [11] model; (c-d) Cropped image size 128×128 and 64×64 ; (e-f) Segmentation by [11] model; (g-h) Successful segmentation of the object with the New model.

segmentation and the other for local and selective segmentation) for reliable segmentation, improving on two related models proposed recently. Numerical experiments show that the new model delivers similar results for easier problems to old models and equally reliable results for harder problems where old models fail. Future work will focus on selective segmentation in higher dimensions and on fast algorithms development.

References

- [1] D. Adalsteinsson and J. A. Sethian, A fast level set method for propagating interfaces, *J. Comput. Phys.*, 118(2) (1995), 269–277.
- [2] R. Adams and L. Bischof, Seeded region growing, *IEEE T. Pattern Anal.*, 16(6) (1994), 641–647.
- [3] G. Aubert and P. Kornprobst, *Mathematical Problems in Image Processing*, Springer, New York, 2002.
- [4] N. Badshah and K. Chen, Image selective segmentation under geometrical constraints using an active contour approach, *Commun. Comput. Phys.*, 7(4) (2009), 759–778.
- [5] X. Bresson, S. Esedoglu, P. Vandergheynst, J. P. Thiran and S. Osher, Fast global minimization of the active contour/snake model, *J. Math. Imag. Vision*, 28(2) (2007), 151–167.
- [6] V. Caselles, R. Kimmel and G. Sapiro, Geodesic active contours, *Int. J. Comput. Vision*, 22(1) (1997), 61–79.
- [7] T. F. Chan, B. Y. Sandberg and L. A. Vese, Active contours without edges for vector-valued images, *J. Vis. Commun. Image Rep.*, 11(2) (2000), 130–141.
- [8] T. F. Chan and J. H. Shen, *Image Processing and Analysis-Variational, PDE, Wavelet and Stochastic Methods*, SIAM Publications, Philadelphia, USA, 2005.
- [9] T. F. Chan and L. A. Vese, Active contours without edges, *CAM Report, UCLA* (98-53), (1998).
- [10] T. F. Chan and L. A. Vese, An efficient variational multiphase motion for the Mumford-Shah segmentation model, *Proc. 34th Asilomar Conf. Signals, Systems and Computers*, 1 (2000), 490–494.
- [11] T. F. Chan and L. A. Vese, Active coutours without edges, *IEEE Trans. Image Proc.*, 10(2) (2001), 266–277.
- [12] N. Forcadel, C. Le Guyader and C. Gout, Image segmentation using a generalized fast marching method, *Numer. Algor.*, 48(2) (2008), 189–212.
- [13] C. Gout, C. Le Guyader and L. Vese, Segmentation under geometrical conditions with geodesic active contour and interpolation using level set methods, *Numer. Algor.*, 39 (2005), 155–173.
- [14] C. Le Guyader and C. Gout, Geodesic active contour under geometrical conditions theory and 3D applications, *Numer. Algor.*, 48 (2008), 105–133.
- [15] C. Gout and C. Le Guyader, Segmentation of complex geophysical structures with well data, *Comput. Geosci.*, 10(4) (2006), 361–372.
- [16] M. Kass, A. Witkin and D. Terzopoulos, Snakes: active contour models, *Int. J. Comput. Vis.*, 1 (1987), 321–331.
- [17] S. Kichenassamy, A. Kumar, P. Olver and A. Yezzi, Snake: conformal curvature flows: from phase transitions to active vision, *Arch. Ration. Mech. An.*, 134(3) (1996), 275–301.
- [18] C. Li, C. Xu, C. Gui and M. D. Fox, Level set evolution without re-initialization: a new variational formulation, *IEEE Computer Society Conference on Computer Vision and Pattern Recognition*, 1 (2005), 430–436.
- [19] F. Li, M. K. Ng, T. Y. Zeng and C. L. Shen, A multiphase image segmentation method based on fuzzy region competition, *SIAM J. Image Sci.*, 3(3) (2010), 277–299.
- [20] T. Lu, P. Neittaanmäki and X.-C. Tai, A parallel splitting up method and its application to Navier-Stokes equations, *Appl. Math. Lett.*, 4(2) (1991), 25–29.
- [21] J. Malik, Th. Leung and J. Shi, Contour and texture analysis for image segmentation, *Int. J. Comput. Vision*, 43(1) (2001), 7–27.

- [22] A. Mitiche and I. Ben-Ayed, *Variational and Level Set Methods in Image Segmentation*, Springer-Verlag, 2010.
- [23] R. Malladi, J. A. Sethian, and B. C. Vermuri, A fast level set based algorithm for topology independent shape modeling, *J. Math. Imag. Vision*, 6 (1996), 269–289.
- [24] D. Mumford and J. Shah, Optimal approximation by piecewise smooth functions and associated variational problem, *Commun. Pure Appl. Math.*, 42 (1989), 577–685.
- [25] S. Osher and R. Fedkiw, *Level Set Methods and Dynamic Implicit Surfaces*, Springer, Berlin, 2003.
- [26] R. Ronfard, Region-based strategies for active contour models, *Int. J. Comput. Vis.*, 13 (1994), 229–251.
- [27] J. A. Sethian, Fast marching methods, *SIAM Rev.*, 41(2) (1999), 199–235.
- [28] J. A. Sethian, *Level Set Methods and Fast Marching Methods: Evolving Interfaces in Computational Geometry, Fluid Mechanics, Computer Vision and Material Science* (Cambridge Univ. Press, London, 1999).
- [29] D. Sen and S. K. Pal, Histogram thresholding using fuzzy and rough measures of association error, *IEEE Trans. Image Pro.*, 18(4) (2009), 879–888.
- [30] W. B. Tao and X.-C. Tai, Multiple piecewise constant active contours for image segmentation using graph cuts optimization, *UCLA CAM report 09-13*, (2009).
- [31] L. A. Vese and T. F. Chan, A multiphase level set framework for image segmentation using the mumford and shah model, *Int. J. Comput. Vision*, 50(3) (2002), 271–293.
- [32] C. Vincent and P. Soille, Watersheds in digital spaces: an efficient algorithm based on immersion simulations, *IEEE Trans. Patten Anal.*, 13 (1991), 583–598.
- [33] J. Weickert and G. Kuhne, Fast methods for implicit active contour models, *Geometric Level Set Methodes in "Imaging, Vision and Graphics"*, pp. 43–58, eds. S. Osher and N. Paragios, Springer, 2003.
- [34] J. Weickert, B. M. ter Haar Romeny and M. A. Viergever, Efficient and reliable schemes for nonlinear diffusion filtering, *IEEE Trans. Image Proc.*, 7(3) (1998), 398–410.
- [35] S. W. Zucker, Region growing: childhood and adolescence, *Comput. Graph. Image Proc.*, 5 (1976), 382–399.